NUMERICAL MODELLING OF DRY FRICTION OF PISTON RINGS IN INTERNAL COMBUSTION ENGINES

Peter Raffai[1], Ondřej Maršálek[2], Gabriela Nečasová[3]

Summary: The aim of the article is to experimentally evaluate the contact area and to compare the measured results with different contact model theories. The experiment takes advantage of the electrical contact resistivity principle in a dry piston/cylinder liner test rig assembly. Analytical contact models are implemented into the computational simulation. The calculated contact area depends on the dynamics and precomputed database of contact pressure and contact area in relation to the separation distance of surfaces.

Key words: Contact pressure, Multi-Body System (MBS), Rough surface, Contact resistivity.

INTRODUCTION

Even though the number of cars and trucks with electric or other alternative engines is rising, the internal combustion engines still dominate the market. According to the current research on the reserves of fossil fuels (oil, natural gas), this domination is going to last at least another 20 years. Therefore, due to stringent emission standards, further research and development of internal combustion engines is very important. The current aim of the research can be separated into three main areas: recuperation of energy from the exhaust, development of new strategies to maximise the effectiveness of the engine and development of affordable devices to treat the composition of exhaust gases. The decrease of the frictional losses is directly linked to the last area.

One of the possibilities of decreasing the friction is to decrease the friction coefficient between the touching machine parts (so-called tribological pairs). The low emission limits of current and planned norms force the developers to focus on less explored tribological pairs, such as piston rings and cylinder liner. New techniques for surface treatment and application of new surface coatings allow for more combinations of touching surfaces. These new combinations can change the frictional properties however, the amount of change and possible improvement have to be investigated. In the case of known input parameters, the investigation can be carried out using computer simulation. Otherwise, technical experiments have to be carried out.

1. ANALYTICAL CONTACT MODELS

This chapter introduces all of the theoretical models for the contact pressure

[1] Ing. Peter Raffai, Brno University of Technology, Faculty of Mechanical Engineering, Technická 2896/2, 616 69, Brno, Czech Republic, Tel: +420 541 143 476, E-mail: peter.raffai@vutbr.cz

[2] Ing. Ondřej Maršálek Ph.D., Brno University of Technology, Faculty of Mechanical Engineering, Technická 2896/2, 616 69, Brno, Czech Republic, Tel: +420 541 143 476, email: ondrej.marsalek@vutbr.cz

[3] Ing. Gabriela Nečasová, Brno University of Technology, Faculty of Information Technology, Božetěchova 2, 612 66, Brno, Czech Republic, Tel: +420 541 141 270, E-mail: inecasova@fit.vutbr.cz

calculation, which were considered in the developed complex algorithm for detailed analysis of rough surfaces.

1.1 Contact Model by Greenwood & Tripp

The first contact model is by Greenwood & Tripp (1), published in 1970. It is very time-effective and widely used model. The governing equation for the contact pressure calculation can be written as:

$$p_{c(h)} = \frac{8\pi}{5}\left(\eta_{r\beta\sigma}\right)KF_{5/2}\left(\frac{h}{\sigma}\right) \quad (1)$$

where

$$K = \frac{2\sqrt{\{2\}}}{3}(\eta_r\beta\sigma)E'\sqrt{\left(\frac{\sigma}{\beta}\right)}, \quad (2)$$

$$\sigma = \sqrt{Sq_1^2 + Sq_2^2}, \quad (3)$$

$$\frac{1}{E'} = \frac{1-v_1^2}{E_1} + \frac{1-v_2^2}{E_2}, \quad (4)$$

where η_r is the surface density of roughness peaks $[m^{-2}]$, h is the oil film height (distance between mean planes of 3D rough surface profiles) $[m]$, β is the average radius of curvature of rough surface asperities $[m]$, σ is the combined RMS of both surfaces $[m]$, v is the Poisson's ratio [-], Sq is the root mean square of a 3D rough profile $[m]$, E' is the combined Young's modulus $[Pa]$, $E_{1(2)}$ is Young's modulus for each material of the contact pair $[Pa]$ and $F_{5/2}$ is the function of contact pressure increase [-]. Function $F_{5/2}\left(\frac{h}{\sigma}\right)$ is given by the table in information source (1). From equation (1) it can be observed, that this variable depends only on the $\frac{h}{\sigma}$ ratio and it is necessary to determine the value of this function for all (h/σ) ratios which occur during simulation.

The values of function $F_{5/2}\left(\frac{h}{\sigma}\right)$ can be obtained by an interpolating polynomial of $(n_{F_{5/2}} - 1)$-degree, where $n_{F_{5/2}}$ is the overall number of the table values of contact pressure increase. The table is given by nine values and therefore an eight-degree interpolating polynomial was applied. Coefficients (in double precision format, see Table 1) of this polynomial are obtained from MATLAB programming environment.

1.2 Contact Model by Hertz

Probably the most widely known and most widely used contact model is by Hertz. Accepted simplifying assumptions (taken from source (2)) are: contact bodies are considered isotropic, elastic and perfectly smooth. The contact area is considered small and flat in comparison with the radius of curvature of undeformed contact bodies.

In the case of analysis of contact of two 3D rough surfaces, it seems to be convenient to replace the real shape of surface asperities with an ideally spherical shape. The Hertzian pressure is then solved as a contact of two spherical bodies. The contact force W $[N]$ is calculated as:

$$W = \sqrt{\frac{\delta_R^3 E'^2 R'}{1.0397^3}}. \quad (5)$$

Here δ_R is the deflection (penetration) of surfaces $[m]$, E' is the combined Young's modulus $[Pa]$ and R' is the combined radius of curvature $[m]$. The radius of contact area a $[m]$ is given by the equation:

$$a = \left(\frac{3WR'}{E'}\right)^{\frac{1}{3}}. \quad (6)$$

Equations for the determination of maximal (P_{max}) and average (P_{av}) contact pressure $[Pa]$ follows.

$$P_{max} = \frac{3W}{2\pi a^2}, P_{av} = \frac{W}{\pi a^2}. \quad (7)$$

Input variables for this contact model are then the deflection (penetration) of contact bodies δ_R $[m]$, the material characteristic Young's modulus E' $[Pa]$ and the combined radius of curvature R' $[m]$.

For all contact models (except the model by Greenwood & Tripp) an identical way of combined radius of rough surfaces curvature calculation is used. This calculation is based on the determination of the osculation circle's radius. This radius of curvature is determined for each point of a surface rough profile in both directions (x and y). The radius of curvature of contact body 1 in direction x is given by the equation:

$$R_{1x} = \frac{\left(1+\left(z_r'(x)\right)^2\right)^{3/2}}{z_r''(x)}. \quad (8)$$

1.3 Contact Model by Lagemann

Slightly modified equations for Hertzian pressure calculation were published by Lagemann (3).

$$P_{max} = \frac{1}{\pi}\sqrt{\frac{6E'^2 W}{R'^2}} \quad (9)$$

The combined Young's modulus and the combined (reduced) radius of curvature of contact bodies are described by identical formulae, as in the case of the above-mentioned Hertzian contact model. The radius of the contact area a $[m]$ is calculated differently. This calculation is governed by the following formula:

$$a = \left(\frac{3WR'}{4E'}\right)^{\frac{1}{3}}. \tag{10}$$

The normally acting contact force W $[N]$ is also calculated according to a different formula:

$$W = \sqrt{\frac{16\delta_R^3 E'^2 R'}{9}}. \tag{11}$$

The average contact pressure P_{av} $[Pa]$ is then given by the penetration of the surfaces:

$$P_{av} = P_{max}\sqrt{1 + \frac{distance^2}{a^2}}. \tag{12}$$

1.4 Contact Model by Pasaribu & Shipper

This computational model (4) takes into consideration all three possible states of material behaviour – fully elastic, elastoplastic, and fully plastic behaviour. When compared to all previous models, only one extra variable is added – hardness of the softer material. Transitions between the individual material behaviours are controlled by the depth of the penetration. Boundary values of penetration (deflection) (ω_c [-]) are given by the following equations:

$$\omega_{c1} = 0.89R'\left(\frac{H_m}{E'}\right), \tag{13}$$

$$\omega_{c2} = 54\omega_{c1}. \tag{14}$$

The contact behaves elastically when the condition of $\delta_R < \omega_{c1}$ is met. The elastoplastic behaviour of the contact pair is considered in the case when the condition of $\omega_{c1} < \delta_R < \omega_{c2}$ is valid. And finally – the condition for fully plastic behaviour is given by the relation $\omega_{c2} < \delta_R$.
In the case of fully elastic behaviour the calculation is governed by the formulae:

$$A_{el} = \pi R'\delta_R, \tag{15}$$

$$F_{el} = \frac{4}{3}E'R'^{0.5}\delta^{R1.5}. \tag{16}$$

If materials are in the region of elastoplastic behaviour (the second condition is met) the calculation uses the following formulae:

$$A_{ep} = \pi R' \delta_R \left[1 - 2\left(\frac{\delta_R - \omega_{c1}}{\omega_{c2} - \omega_{c1}}\right)^3 + 3\left(\frac{\delta_R - \omega_{c1}}{\omega_{c2} - \omega_{c1}}\right)^2\right], \quad (17)$$

$$F_{ep} = \left[H_m - 0.6H_m \frac{\ln \omega_{c2} - \ln \delta_R}{\ln \omega_{c2} - \ln \omega_{c1}}\right] A_{ep}. \quad (18)$$

And finally – equations describing the fully plastic behaviour of the contact pair have the following shape:

$$A_{ep} = 2\pi R' \delta_R, \quad (20)$$

$$F_p = H_m A_p. \quad (21)$$

Here A_{el}, A_{ep} and A_p are contact areas $[m^2]$ for given material states, H is the hardness of the softer material $[Pa]$, and F_{el}, F_{ep} a F_p are contact forces $[N]$.
The integral contact pressure in all described cases is calculated as the sum of contact forces applied on the area of the analysed surface element.

2. EXPERIMANTVAL VALIDATION

2.1 Multi-Body System Model

To compare the experiment with one of the contact theories, the computational model needs to be created.

From the macroscopic point of view, if the two round shaped contacting bodies are rigid, only a single force will act upon the single point of contact. In the different case of flexible bodies, the contact region will widen and cause the contact force to spread as it is shown in Figure 1. Moreover, the deformation is not only in the region of the contact force applied present. The deflection of one node affects its adjacent neighbours as well. The overall size of the contact area is evaluated as the total sum of elements active in the contact. This approach is greatly supported by the finite element method.

On the other hand, from the microscopic point of view, the contact forces between two rough surfaces are carried by its asperities (Figure 1). As previously mentioned, considering the two contacting bodies as rigid, while the asperities can locally deform. Contact forces result in a deformation of each active asperity. The number of asperities in contact, the contact pressure and the size of the overall contact area are, therefore, dependent on the nominal surface distance h. Global elastic (plastic) deformation of bodies affects this nominal surface distance.

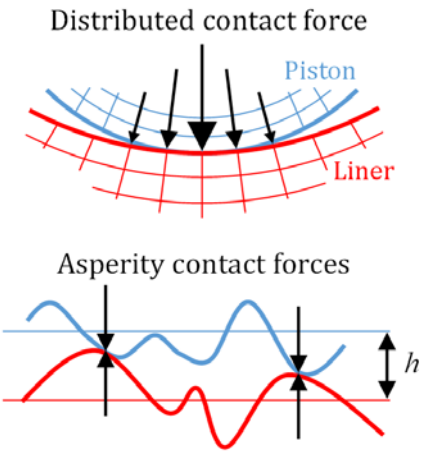

Source: Author

Fig. 1 - Contact of two flat flexible bodies and rough surface contact

A database of contact pressure depending on the analysed surfaces separation was created for this MBS simulation. Shapes of individual curves are shown in the following figure.

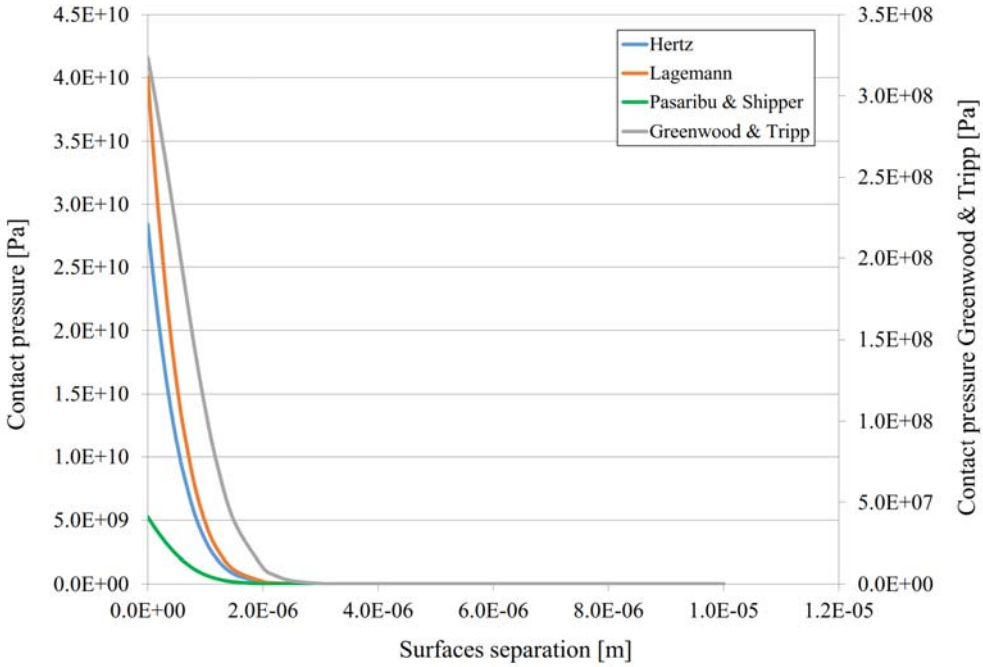

Source: Author

Fig. 2 - Contact pressure depending on surfaces separation

Taking into account the presumed loads of contact pair, only elastic deformations of both parts are presumed. Therefore, for the MBS simulations, only rigid bodies were used. For the MBS simulation a commercially available software tool – ADAMS – was used.

A simple diagram of MBS simulation functionality is shown in the next figure. MBS simulation works as an actual experiment.

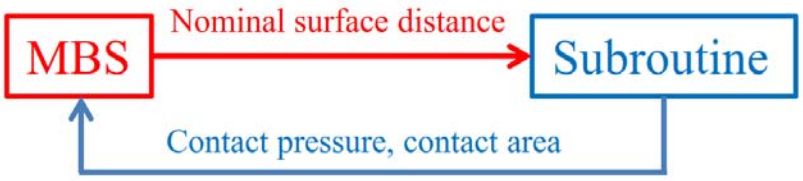

Source: Author

Fig. 3 - Diagram of MBS simulation functionality

Each node of the computational mesh represents an area of one element. If one element is represented by one node, the nominal distance between two elements is constant over the whole area of the element. These presumptions, to keep sufficient accuracy of simulation results, require relatively dense computational mesh. For this purpose, variable mesh density was applied, taking into consideration the presumed areas of contact. This approach allows maintaining high precision of calculation together with sufficient time efficiency of the developed algorithm. To suppress piston oscillation a damping force was applied. The final force acting in the normal direction is given by the following formula:

$$F_{c_{MBS}} = P_c A_c - B_{MBS} v_{MBS}, \tag{22}$$

where F_{cMBS} is the contact force $[N]$, Pc is the contact pressure $[Pa]$, Ac is the contact area $[m^2]$, BMBS is damping $[N \cdot s \cdot m^{-1}]$, and v is the relative velocity of surfaces $[m \cdot s^{-1}]$. `This model` then simulates a static equilibrium between piston and piston liner without any relative movement between piston and piston liner in the direction of piston axis.

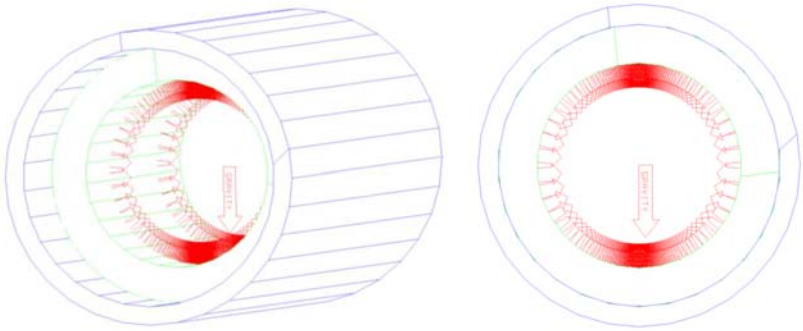

Source: Author

Fig. 4 - Variable density of computational mesh

2.2 Measuring Circuit Design

By using a simple equation, described in the reference (4), it is possible to preliminarily suggest values of voltage and electric current in the measuring circuit.

$$R_T = \frac{\zeta h_R}{A_R} \tag{23}$$

Where R_T is the contact resistance between piston and piston liner $[\Omega]$, A_R is the contact pressure $[m^2]$, hR is the electric contact height $[m]$, and ζ is the material resistance $[\Omega m]$.

The overall (simplified) resistance in this circuit is given by the sum of these contact resistances, the resistance of conductors, other contact resistances and the resistance of each body. This resistance is possible to determine by the use of equation (23). A contact height h_R is here substituted by the height of the piston liner (piston) wall.

$$I = \frac{U_R}{R_T + R_{piston} + R_{pistonLiner}} \tag{24}$$

The resulting current is quite high. For this reason, it is necessary to integrate an additional resistor of a known value (in our case $100\ \Omega$), which causes the decrease in the value of electric current going through the electric circuit. Electric current, reduced this way, then has a value of $1.2.10^{-1}\ A$ $(120\ mA)$, which is an acceptable value (the electric current the source is limited to a value of $1A$). Furthermore, by using a formula:

$$U_c = R_T \cdot I. \tag{25}$$

The value of voltage in the piston/piston liner contact $U_c = 1.3410^{-8}\ V$. To record this value $(13.4\ nV)$ a very precise measuring device (nanovoltmeter together with a stable source of electric current) is required. The design of both main parts does not allow to separately measure only the transitional resistance. It is possible to measure only the resistance (or voltage) of the whole circuit (resistance of all bodies and contacts in the electrical circuit).

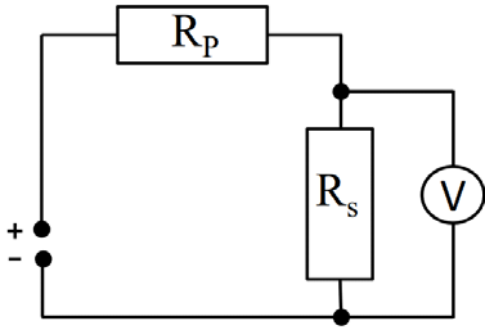

Source: Author

Fig. 5 - Primarily designed electrical scheme:
R_P – added resistance
R_s – associated resistor (resistance of the contacts + resistance of conductors and bodies)

The intentionally chosen design of the experimental piston allows inserting a weight into the piston body. Thus, it is possible to gradually change the acting force between piston and piston liner and to observe the contact area changes. When the measuring circuit was finished, greater (than predicted) values of resistivity were measured. Therefore, it was possible to remove the additional resistor.

The experimental device was designed according to Figure 5. Crankshaft motion was constrained so the experiment could be performed as the simplest scenario. The intentionally chosen design of the experimental piston allows the insertion of a weight inside the piston body. Thus, it is possible to gradually change the acting force between the piston and piston

liner and to observe the contact area changes.

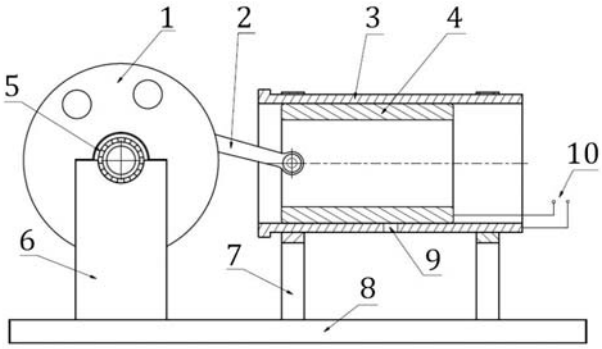

Source: Author

Fig. 8 - Test rig scheme: 1 – crankshaft powered by electric engine, 2 – connecting rod, 3 – piston liner, 4 – experimental engine, 5 – crankshaft mount, 6 – crankshaft bearing housing, 7 – piston liner support, 8 – base, 9 – oil intake, 10 – cables for electric circuit connection.

2.3 Experimental Results

Measuring was done with the device Keithley 6221/2182A Delta mode system with AC and DC current source and nanovoltmeter.

Tab. 1 - Measured values of electrical contact resistance

Weight [kg]	R_T [mΩ]						
	M1	M2	M3	M4	M5	M6	Avg
5.4400	7.1124	9.5167	6.6582	7.8624	8.7874	8.6104	8.0913
7.4400	6.5575	9.1613	5.9213	7.2133	8.3133	7.9753	7.5237
10.5260	4.4391	6.4177	5.8974	5.5848	6.3048	7.0488	5.9488
13.6160	3.8703	5.0967	4.6878	4.5516	5.2016	5.1416	4.7583
16.7080	3.3107	4.2789	3.6717	3.7537	4.4537	4.3717	3.9734
19.7950	2.7483	3.6219	3.3810	3.2504	3.5504	3.8704	3.4037
22.8820	2.1726	2.3192	2.0260	2.1726	2.4726	2.5866	2.2916
25.9660	1.7723	1.4934	2.0512	1.7723	1.9723	2.0123	1.8456

Source: Author

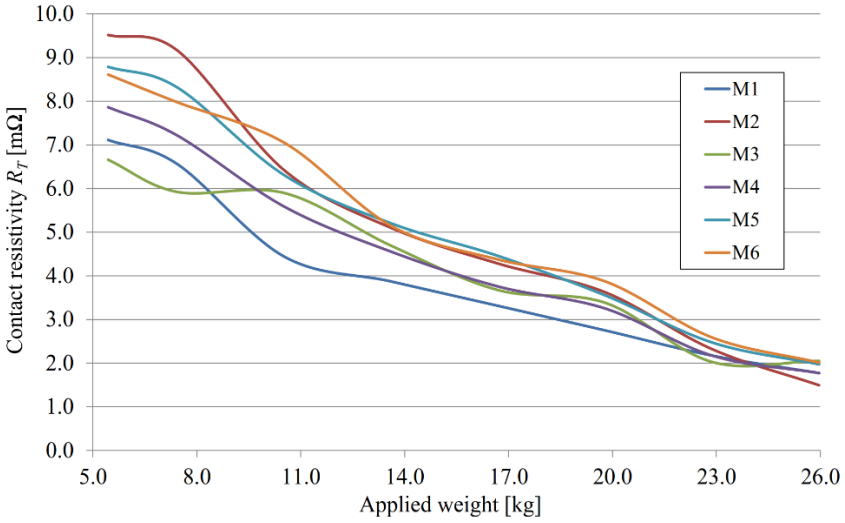

Source: Author

Fig. 9 - Contact resistance on applied weight dependence

Source: (2)

Fig. 10 - Current source and nanovoltmeter Keythley

From the measured values, it is possible to observe great difference when compared to the predicted values. These differences are caused (as was partially mentioned above) by:

- different resistances of both materials,
- different resistances of conductors,
- different resistances of transitional resistors,
- the different transitional resistance of contact (oxidation/contamination of surface layers),
- and others.

The following graph shows the results of the numerical simulation of contact between piston and piston liner. Applied weights were similar to the weights of the actual experiment.

Source: Author

Fig. 11 - Results of the piston/piston liner contact MBS simulation

The conversion of contact area to the transitional resistance can be done by the above mentioned formula. The following graph presents curves representing ratios of each transitional resistance to its first value. It allows the comparison of measured curves with the calculated curves. This is the reason why all curves start from the same value, the value of 1.

Source: Author

Fig. 12 - Comparison of results from MBS simulation with results from experiment

By looking at the graph, it is possible to state that this way of contact area measuring is useable and the functionality of this principle was validated.

Simultaneously, it is necessary to think about that fact that this graph does not provide unequivocal information about which of the analytical approaches is the closest to results from measuring – this is a logical assumption. The maximum force (weight) applied to the piston was about $255\ N\ (26\ kg)$.

It is possible to state that results are in the area of low elastic deformations. All of the implemented contact models give very similar results in this area (three out of four are based on the Hertzian theory for the elastic behaviour). To obtain results which would be better in revealing the differences between individual computational models, the use of simpler test samples would be necessary (geometrically), and would have to apply forces causing deformations from the whole range (from elastic to the plastic deformations). For this purpose, for example, the hydraulic press seems to be suitable.

The complexity of the whole problem shows that the evaluation of contact area, using a similar experiment that is outlined here, would cover a topic for a single doctoral thesis. The result of the functionality of this principle described here, together with the work done so far, can be used as a base for further work in this area.

The complete experimental device is equipped with highly sensitive sensors of distance, complex lubricating condition, and, for example, also with a crank mechanism to create a straightforward reciprocating movement of the piston in the piston liner. This experimental device is going to be further developed independently from this thesis. It is going to be used for the experimental evaluation of a computational model of lubrication height between piston and piston liner.

Taking into consideration the need to choose from analytical contact models, the further methodology was suggested for this purpose. It is a possibility to use the commercially available, well-known software tool ANSYS.

3. CONCLUSION

The designed test rig was, in this case, focused on the dry contact of piston/cylinder liner. The change in electrical contact resistance was able to record the differences in the contact area due to various loads applied, even when only very low elastic deformations were present – the measuring principle using contact resistance was proven.

Experimental and simulated data have similar trends, but the offset is significant. It is caused by the unknown resistance between the individual measuring circuit items. At this moment, the best from the selected analytical contact models cannot be determined. For this purpose, higher deformations would have to be introduced. Further development of the test rig leading to the successful continuation of the experiment is suggested.

4. ACKNOWLEDGEMENT

The research leading to these results has received funding from the Brno University of Technology (Project FIT/FSI-J-16-3689). This support is greatly appreciated.

REFERENCES

(1) GREENWOOD, J. A. and TRIPP, J. H. The Contact of Two Nominally Flat Rough Surfaces. *Proceedings of the Institution of Mechanical Engineers.* 1970. vol. 185, no. 1, p. 625-634. DOI10.1243/PIME_PROC_1970_185_069_02.

(2) STACHOWIAK, G. and BATCHELOR, A. *Engineering Tribology*. 4th ed. Amsterdam: Elsevier Butterworth-Heinemann, 2014. ISBN 07-506-7836-4.

(3) LAGEMANN, V. *Numerische Verfahren zur tribologischen Charakterisierung bearbeitungsbedingter rauher Oberflächen bei Mikrohydrodynamik und Mischreibung.* Dissertation. Kassel (Germany), 2000.

(4) PASARIBU, H. R. and SCHIPPER, D. J. Application of a Deterministic Contact Model to Analyze the Contact of a Rough Surface Against a Flat Layered Surface. *Journal of Tribology*. 2005. vol. 127, no. 2, p. 451-455. DOI 10.1115/1.1866163.